Advanced Dynamic Simulation of Supercapacitors Considering Parameter Variation and Self-Discharge

Sang-Hyun Kim, Woojin Choi, *Member, IEEE*, Kyo-Bum Lee, *Senior Member, IEEE*, and Sewan Choi, *Senior Member, IEEE*

***Abstract*—In this paper, dynamic simulation of the equivalent circuit model of the supercapacitor, taking into account the parameter variations and self-discharge, is discussed. Self-discharge is modeled with equivalent impedance including a constant phase element (CPE), and the parameter variations depending on the voltage are reflected. Since it is difficult to directly simulate the ZARC element (*R*-CPE parallel circuit) with a circuit simulation tool such as the professional simulation program with integrated circuit emphasis (PSPICE), equivalent transformation to three *R-C* parallel circuits is introduced in the simulation. The accuracy of simulation with the model is then verified through a comparison with results of an experiment. The comparison shows that the model using a CPE is effective in representing the dynamic characteristics and self-discharge of supercapacitors. Accordingly, it proves that the method proposed in this study can be useful in developing systems that include supercapacitors, and can be applied in an integrated simulation of a supercapacitor and a power electronic system.**

***Index Terms*—Dynamic simulation, electrochemical impedance spectroscopy, equivalent circuit, self-discharge, supercapacitor.**

I. Introduction

Because of their high-power density, long cycle life, and clean nature, supercapacitors are used to improve the dynamic characteristics of power sources that have slow responses and to protect them from overload. Supercapacitors have been widely used in various applications in combination with power electronic circuits [1]–[7]. Power electronic systems are becoming ever more complicated, and simulation-based development methods are often used in developing such systems to find better system architectures and optimal operation strategies. In such cases, accurate modeling is crucial for all components, and supercapacitors, in particular, require a comprehensive model that is developed after a thorough understanding of its internal structure and characteristics. For this purpose, there have been many attempts to electrically model the distinct characteristics of supercapacitors [8]–[13].

The simplest of the electric equivalent impedance models of supercapacitors is an equivalent series resistance connected with a capacitor in series. The benefits of the model include its ease of interpretation and simulation; however, it does not properly represent the physical structure of supercapacitors, making it impossible to accurately describe charge/discharge and self-discharge behaviors. Models that are more advanced were developed in some studies, but they are also not enough to effectively reflect characteristics of the porous electrodes and ion movements within the supercapacitors, resulting in discrepancies between simulation and experimental results.

The electric model for supercapacitors with porous electrodes was first introduced by De Levie; this model shows equivalent impedance of porous electrodes as a ladder circuit of resistances and capacitors [14]. Buller applied such a porous-electrode model to a supercapacitor model and proposed an *R-C* parallel-branch model for the dynamic simulations with Matlab/Simulink; this model was equivalently transformed from De Levie's porous electrode model, which has been prevalently used thus far [8]. However, Buller's model excludes the self-discharge phenomenon that affects the static and dynamic characteristics of supercapacitors, and thus, there are likely to be discrepancies between experiment and simulation results. Efforts have been made by Diab and Kaus to model the self-discharge of the supercapacitor by the variation of conventional equivalent impedance model of the supercapacitor to account for the self-discharge phenomenon [12], [13]. Diab employed a relatively simple R-C series circuit for modeling the self-discharge and the circuit elements were experimentally determined according to the self-discharge time behavior. Kaus established a complex electrical model to account for the effect of the charge redistribution during self-discharge and it was capable of predicting the effects of charge duration, initial voltage, and temperature on the open circuit voltage decay. Supercapacitor have a higher tendency for self-discharge compared to secondary batteries, and during the pause period (i.e., during stoppage in charge/discharge), the voltage depends on the degree of self-discharge. Developing a model that can explain self-discharge is thus crucial in acquiring accurate simulation results, in case there is a pause period in the simulation, for example, in simulation of driving cycles of fuel cell vehicles or electric cars. Therefore, for an accurate dynamic simulation of supercapacitors, it is necessary to apply self-discharge and parameter variations of the impedance circuit depending on the voltage in the simulation process, although there have been only few simulation studies that consider all the aforementioned factors.

Manuscript received August 18, 2010; revised February 4, 2011; accepted March 19, 2011. Date of current version November 18, 2011. This work has been supported by KESRI (2008T100100162), which is funded by Ministry of Knowledge Economy (MKE). Recommended for publication by Associate Editor F. Wang.

S.-H. Kim and W. Choi are with the Department of Electrical Engineering, Soongsil University, 511 Sangdo-Dong, Dongjak-Gu, Seoul 156-743, Republic of Korea (e-mail: hyun714@poscoict.com, cwj777@ssu.ac.kr).

K.-B. Lee is with the Division of Electrical and Computer Engineering, Ajou University, San5, Woncheon-dong, Yeongtong-gu, Suwon 443–749, Republic of Korea (e-mail: kyl@ajou.ac.kr).

S. Choi is with the Department of Control and Instrumentation Engineering, Seoul National University of Education, 172 Kongneung-Dong, Nowon-Gu, 139–743 Seoul, Republic of Korea (e-mail: schoi@snut.ac.kr).

Color versions of one or more of the figures in this paper are available online at http://ieeexplore.ieee.org.

Digital Object Identifier 10.1109/TPEL.2011.2136388

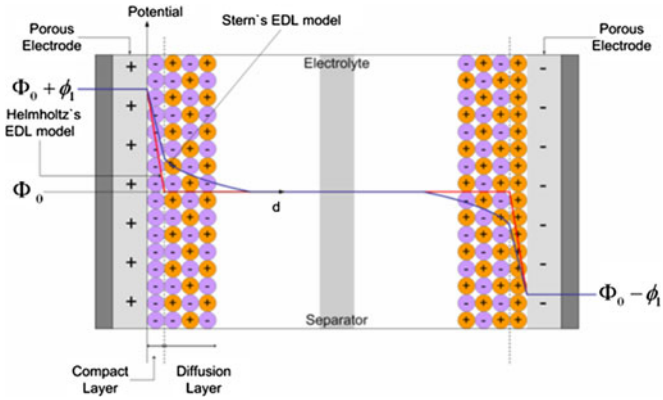

Fig. 1. Internal structure of the supercapacitor.

In this paper, porous electrodes of a supercapacitor are modeled using a ZARC element with a constant phase element (CPE), and the mathematical modeling in the simulation is explained. Also the method for the transformation of ZARC element to three *R-C* parallel circuits is proposed for the simulation with commercially available software. Electrochemical impedance spectroscopy (EIS) was used to acquire parameters of the presented equivalent circuit, and the impedance spectra measured for different voltages were used to extract parameters of the equivalent impedance circuit for different voltages and to model self-discharge. Finally, the developed dynamic model was simulated using Matlab/Simulink, and then, the simulation results and experimental results were compared to prove the validity of the model.

II. Theory

A. Equivalent Circuit Model of Supercapacitor

A supercapacitor is designed with a separator at the middle, porous electrodes on both sides, and an electrolyte between them. The electrolyte consists of solvent and solute that can be ionized. As shown in Fig. 1, negative ions adhere to the positive electrode and positive ions to the negative electrode to store energy. The porous electrodes of a supercapacitor can be expressed as a ladder circuit of an electrolyte resistance in pore (R_e) and an electric double-layer capacitance (C_d) connected in series, as represented by (1) according to De Levie [14]

$$Z_{\text{pore\_ideal}} = \sqrt{\left(\frac{R_e}{j\omega C_d}\right)} \coth \sqrt{j\omega R_e C_d}. \quad (1)$$

The interface of the porous electrode of a supercapacitor is not in an ideal condition, as shown in Fig. 2(a), and (1) is thus insufficient for describing the phenomena of a supercapacitor. Since the interface is in a nonideal condition as shown in Fig. 2(b), it is more appropriate to use a CPE with parameter Q_d and d than to use capacitance to represent the phenomena [15], [16]. R'_e, C'_d, and CPE' are the electrolyte resistance, the electric double-layer capacitance, and constant phase element per unit length (dx) of the pore. In addition, the inductance (series inductance L_s), due to the connection terminals, the sum of contact resistance and ionic resistance (series resistance R_s), and pore

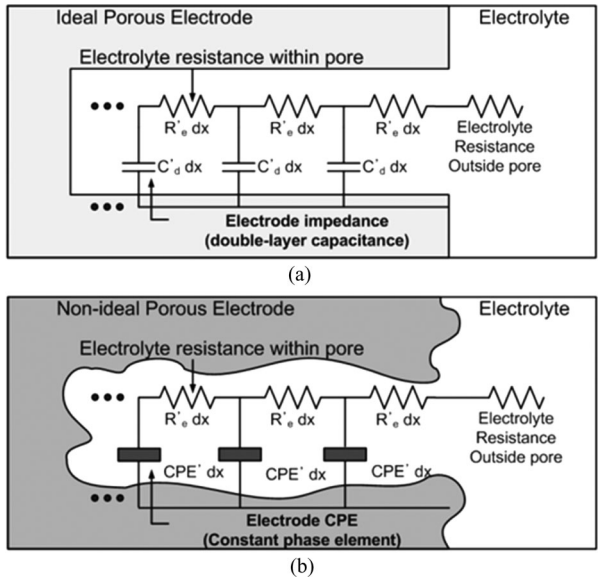

Fig. 2. Model of the ideal porous electrode and nonideal porous electrode. (a) Ideal pore. (b) Non-ideal pore.

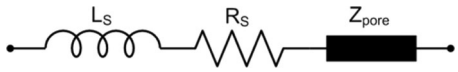

Fig. 3. Equivalent impedance model of the supercapacitor.

impedance (Z_{pore}) can be expressed by the series circuit shown in Fig. 3 and (2) [15], [16]

$$Z_{SC\_\text{nonideal}} = j\omega L_s + R_s + \sqrt{\left(\frac{R_e}{(j\omega)^d Q_d}\right)} \coth \sqrt{(j\omega)^d R_e Q_d}. \quad (2)$$

B. Variation in Capacitance According to the Voltage

Research into the electric double layer (EDL), which is a significant feature of supercapacitors, was initiated by Helmholtz in 1879 and has since been continued by many scholars. The capacitance model developed by Stern in 1924 is now the most commonly used [10]. The capacitance (Cs) of the electric double layer model developed by Stern is represented by the sum of two elements generated by the compact layer and diffusion layer. Specifically, the inverse of Cs is represented as the sum of the inverse of constant capacitance (C_{H}) of the compact layer—also called the Helmholtz layer—and the inverse of Gouy–Chapman capacitance (C_{GC}), which varies depending on the distance between the electrode and ions generated in the diffusion layer, charge voltage, and temperature. This relationship expressed as (3). A variation in the overvoltage (φ) affects the Gouy–Chapman capacitance (C_{GC}), leading to a variation in the capacitance of a supercapacitor. Fig. 1 describes the internal structure of a supercapacitor, which was mentioned above, and the relations between voltage and the distance between the electrode and ions according to the theories of Helmholtz and Stern, where ε is the dielectric constant, A is the area of the

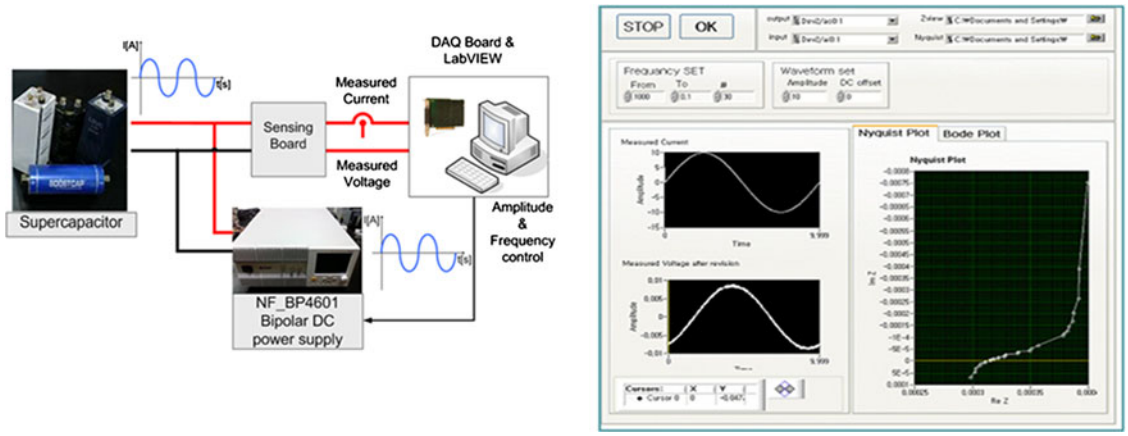

Fig. 4. Experimental setup for the EIS and front panel of the developed software.

electrode, d is the distance between the electrode and ions, z is the ionic charge number, φ, overvoltage, the voltage applied to the electric double layer, c is the density of ions on the electrode surface, R is the gas constant, F is the Faraday constant, and T is the absolute temperature.

$$\frac{1}{C_S} = \frac{1}{C_{\mathrm{H}}} + \frac{1}{C_{\mathrm{GC}}} = \frac{d}{\varepsilon A} + \frac{1}{zFA\sqrt{2\varepsilon c/RT}\cdot\cosh\left(zF\varphi/2RT\right)}. \tag{3}$$

III. EIS Experimental

The voltage-dependent parameters of a supercapacitor were extracted from the impedance spectrum of the supercapacitor obtained by EIS and from curve fitting with an equivalent circuit.

A. Experimental Apparatus for EIS

The impedance of a supercapacitor is so miniscule that it is difficult to measure accurately with a general electrochemical impedance spectrometer with a limited perturbing current of 2 to 3 A. Therefore, an experimental apparatus was designed with an electrochemical impedance spectrometer and software newly developed in our laboratory, as shown in Fig. 4 [17]. A bipolar power supply unit (model BP4610; ±60 V, ±10 A, NF Company) was used for charge/discharge and current perturbation [18]. In the developed system, a sensing circuit, LabVIEW 8.6 software, and PCI-6154 device were used to measure and record the voltage and current of the supercapacitor in real time. The PCI-6154 is a simultaneous sampling multifunction I/O device for PCI bus computers from National Instruments [19]. It is an isolated PCI device featuring four isolated differential 16-bit analog inputs, four isolated 16-bit analog outputs, six DI lines, four DO lines, and two general-purpose 32-bit counter/timers. All A/D converters and D/A converters are capable of 250 kSs^{-1} for each channel. The digitized 16-bit data were sent to the developed software and through the digital lock-in amplifier programmed by LabVIEW 8.6. Signals in the test frequency band were extracted and then the impedance was calculated to draw the impedance spectrum. EIS, a method that perturbs a device and analyzes its response, was performed by limiting the magnitude of the applied perturbation current to below 2% of the charge to ensure linear behavior, as shown in (4), and the quantity of electric charge was kept at a constant level before and after the experiment. The subject of the experiment was a Maxwell Boostcap supercapacitor (2.7 V, 2600 F), and the experiment was conducted at room temperature from 0% V_{rated} to 100% V_{rated} at 20% intervals. The measurement frequencies were between 0.01 Hz and 1 kHz.

$$I_a < 0.02 \times \pi f C_{\mathrm{rated}} V_{\mathrm{rated}}. \tag{4}$$

B. Analysis of Impedance Spectrum by EIS

Fig. 5 shows the results of the EIS experiment at 80% V_{rated}, and those obtained by curve fitting the equivalent circuits of the supercapacitor with the ideal electrode model and with the nonideal electrode model. In the band of high frequency (50 to 0.3 Hz), the results of curve fitting for both models show that as the frequency increases, the impedance plot approaches the asymptotic line that makes an angle of about 45° with the real axis and reaches high-frequency equivalent series resistance (HF ESR), R_s.

In the case of the equivalent circuit of the supercapacitor obtained by the ideal electrode model expressed in (1), when the frequency increased in the band of low frequency, only the imaginary component of the impedance increased, and thus, the impedance curve became perpendicular to the real axis. However, this result differed from the experimental result, which shows the tendency of a slight incline toward the positive real axis.

It was thus found that using the nonideal electrode model involving CPEs is more appropriate, because the real component of the impedance increased a little and the impedance curve tilted slightly toward the positive real axis as the frequency decreased in the band of low frequency, as expressed in (5) [15].

$$Z_{\mathrm{SC\_nonideal}(\omega\to 0)} \cong R_s + \frac{R_e}{3} + \frac{1}{(j\omega)^d Q_d}. \tag{5}$$

As shown in Fig. 5, the result of curve fitting with the nonideal electrode model given in (2) was in accordance with the measurement result of the experiment. Table I gives the parameter

TABLE I
FITTED PARAMETER OF THE SUPERCAPACITOR (80% V_{rated}, 20 °C)

Parameter	L_s (nH)	R_s (mOhm)	R_e (mOhm)	C_d	
Ideal model	65.8	0.329	0.403	2753	
Parameter	L_s (nH)	R_s (mOhm)	R_e (mOhm)	Q_d	d
Non-ideal model	65.8	0.329	0.393	2705	0.9879

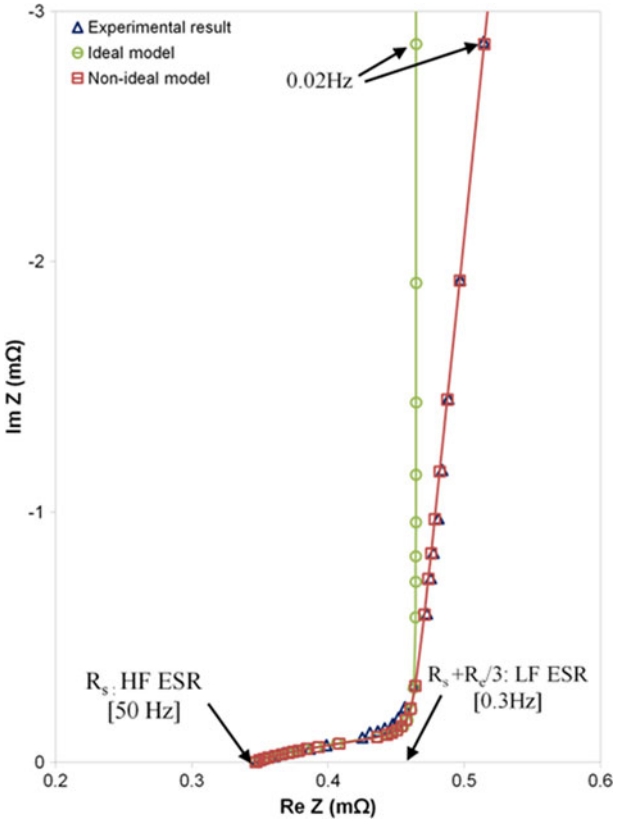

Fig. 5. Nyquist impedance plot of 2.7-V 2600-F Maxwell Boostcap supercapacitor and its fitting result (80% V_{rated}, 20°C).

values obtained by EIS at 80% V_{rated} and by the curve-fitting method for the ideal and nonideal electrode models.

C. Variations in Parameters of Equivalent Circuit According to Voltage

Fig. 6 shows Nyquist impedance plots of the supercapacitor measured from 0% V_{rated} to 100% V_{rated} at 20% intervals. As the electric charge in the supercapacitor increased, the real part of the impedance increased and the absolute value of the imaginary part decreased. This variation in parameter should be reflected to achieve higher accuracy in dynamic simulation. As shown in Fig. 7, the variation in parameter value depending on the voltage was obtained by curve fitting the result shown in Fig. 6, and the variation was expressed as a quadratic equation of the voltage through curve fitting and the accuracy was calculated employing the least-squares method. These results were input into each cycle of the simulation process with Matlab/Simulink, which are detailed in the subsequent Sections IV and V.

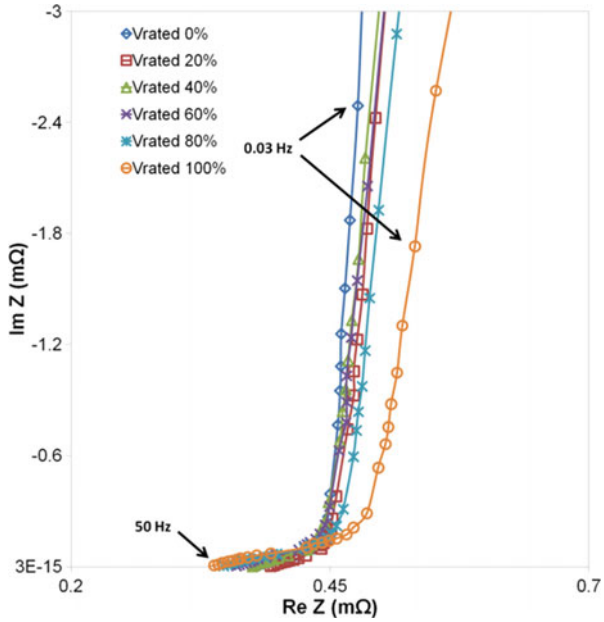

Fig. 6. Nyquist impedance plot of 2.7-V 2600-F Maxwell Boostcap supercapacitor (0–100% V_{rated}).

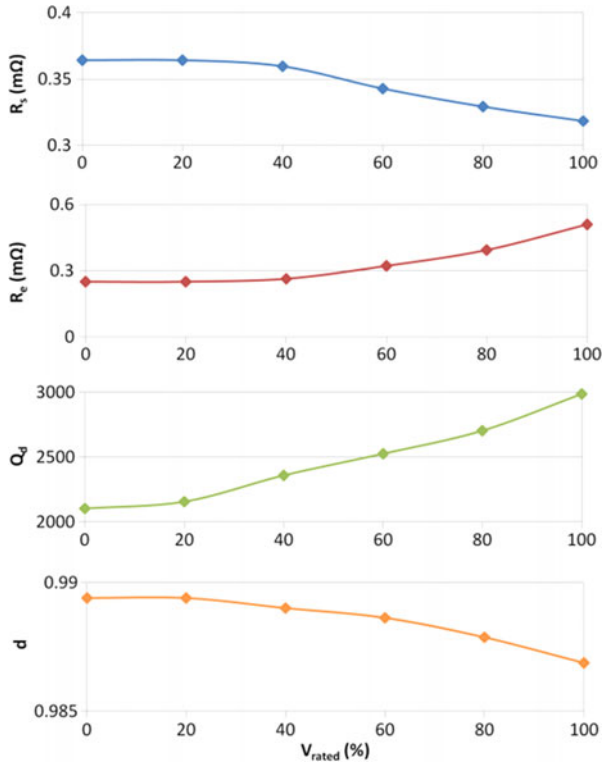

Fig. 7. Variation in parameter values depending on the voltage.

IV. ANALYSIS OF SELF-DISCHARGE OF SUPERCAPACITOR

The self-discharge of supercapacitors has two main causes. First, when a supercapacitor is charged or discharged, there is diffusion of ions from the electrolyte to the electrode, or vice versa. The diffusion, immediately after charge or discharge, causes the self-discharge of supercapacitors. Second, there is

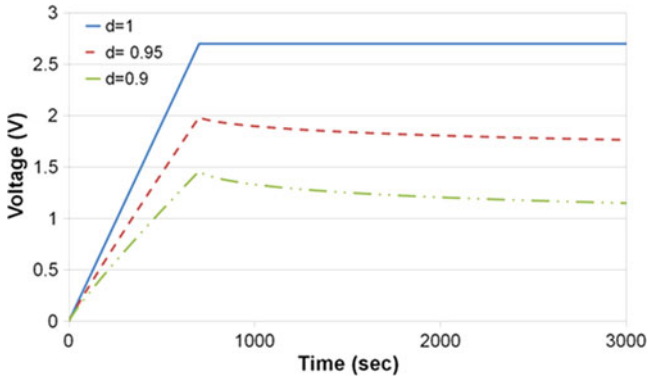

Fig. 8. Simulation of the charge/discharge for different values of coefficient d ($I_c = 10$ A, $C = 2600$ F, ESR $= 0.5$ mΩ).

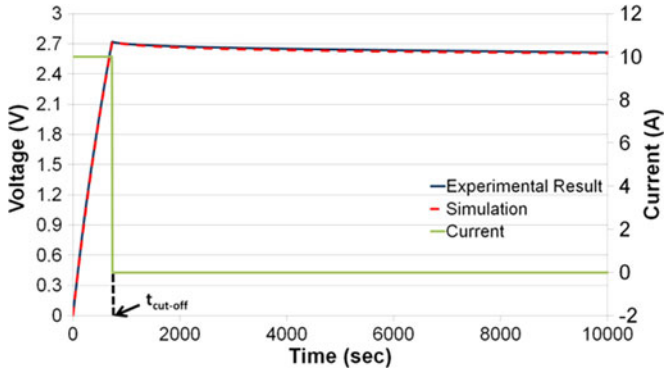

Fig. 9. Experimental and simulation results of the self-discharge response at 100% V_{rated}.

self-discharge due to leakage current, which can be modeled by a leakage resistance connected with a capacitor in parallel. However, self-discharge by diffusion is predominant in the initial stage. The self-discharge by leakage becomes significant some hours after the self-discharge begins [20]. Self-discharge that occurs during dynamic operation, such as the driving cycle of electric vehicles, is thus, thought to be caused mainly by diffusion, which can be explained accurately with a CPE [21]. Since the self-discharge occurs very slowly, the simulation in this study employed the equivalent circuit model of the supercapacitor given by (6), in which the sum (R_s) of contact resistance and ionic resistance was added to the low-frequency model of porous electrodes given in (7).

The response voltage of the supercapacitor can be converted to a function of the time domain and represented by (7) [18]. For the waveform of charge current in the simulation, a step function was used, and (8) was finally used for the simulation, where Γ is the gamma function, I_c the constant current, and H the step function [22].

$$Z_{\text{SC}(\omega\to 0)} \cong R_s + \frac{R_e}{3} + \frac{1}{(j\omega)^d Q_d} \tag{6}$$

$$v_{\text{SC}}(t) = I_c \times \left(R_s + \frac{R_e}{3} + \frac{t^d}{Q_d \cdot \Gamma(1+d)} \right) \tag{7}$$

$$v_{\text{SC}}(t) = I_c \times \left(R_s + \frac{R_e}{3} + \frac{t^d}{Q_d \cdot \Gamma(1+d)} \right) - I_c \times \left(R_s + \frac{R_e}{3} + \frac{(t - t_{\text{cut-off}})^d}{Q_d \cdot \Gamma(1+d)} \right) H(t - t_{\text{cut-off}}). \tag{8}$$

Parameter d has the greatest effect on self-discharge among the parameters of the equivalent impedance circuit of the supercapacitor. Fig. 8 shows the response voltage, simulated using (8) for various values of d, 704 s after a current of 10 A was supplied and then cut off; the voltage waveforms of charge and self-discharge were observed to determine how the supercapacitor's response varies when parameter d varies. It was found that the cut-off voltage of charge decreased as d decreased: when $d = 1$, the supercapacitor was fully charged (2.7 V); when $d = 0.95$, the charge was 1.99 V; and when $d = 0.9$, the charge was 1.489 V. After the current was cut off, the lower the value of d, the more noticeable the self-discharge phenomenon became; as d approached 1, the nature of a pure capacitor became obvious and self-discharge became less noticeable.

TABLE II
FITTED VARIATION OF PARAMETER OF THE SUPERCAPACITOR

	Equation & Value	Unit	R^2
L_s	65.8	nH	N/A
R_s	$4.97 \times 10^{-5}V^2 - 3.98 \times 10^{-5}V + 2.52 \times 10^{-4}$	mOhm	0.998
R_e	$-5.52 \times 10^{-6}V^2 - 3.69 \times 10^{-6}V + 3.66 \times 10^{-4}$	mOhm	0.998
Q_d	$65.83V^2 + 153.5V + 2093$		0.994
d	$-3.99 \times 10^{-4}V^2 + 1.51 \times 10^{-4}V + 9.89 \times 10^{-1}$		0.998

Fig. 9 shows the voltage measured when the supercapacitor was fully charged with a current of 10 A and then the current was cut off. The measured voltage was compared with the simulation results. The variations in the parameters of the equivalent circuit model depending on the voltage were fed back through the expression given in Table II to each step of the simulation. The simulation results were found to be very similar to those of the experiment, as shown in Fig. 9. Unlike the impedance equivalent circuit of the supercapacitor with the ideal electrode model, the nonideal electrode model with CPEs made it possible to describe self-discharge accurately.

Variations in the charge current and parameters of the equivalent circuit affect self-discharge according to the voltage [23], which can be checked with (8). To check these effects, experiments of self-discharge were conducted under several conditions.

First, the effect of the voltage was examined. A current of 10 A was supplied to charge supercapacitors to different voltages from 0% V_{rated}, and then, the charging connector was removed and the open-circuit voltage measured for 30 000 s. As shown by the experimental results in Fig. 10, the higher the voltage, the more noticeable the self-discharge, which was the same result as in the simulation above (Fig. 8). The reason for the effect is that the parameter d of a CPE decreases as the voltage increases. Therefore, it is obvious that the effect of self-discharge increases as the voltage increases.

Fig. 11 shows experimental results of self-discharge with different charge currents. In the experiments, the charge current

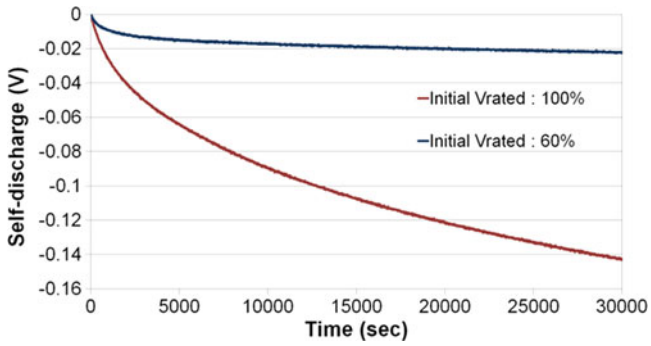

Fig. 10. Self-discharge of supercapacitor for different V_{rated} (100% and 60%).

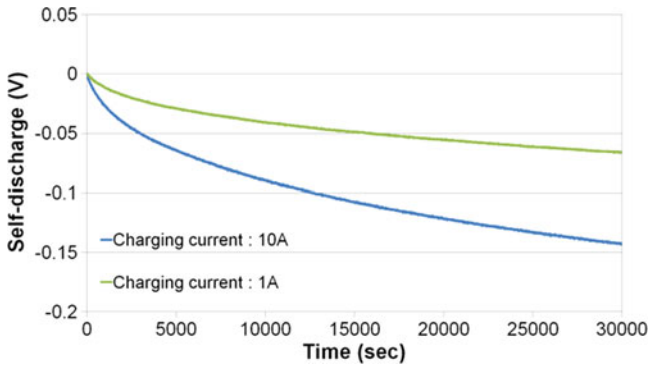

Fig. 11. Self-discharge of supercapacitor for different charging currents (10 and 1 A).

was varied to 10 and 1 A and supplied to fully charge the supercapacitors. After the charging connector was removed, the open-circuit voltage was measured. As shown in the figure, the larger the charge current, the more noticeable the self-discharge.

V. Method of Dynamic Simulation by Matlab/Simulink and Experimental Results

The impedance of porous electrodes with a CPE can accurately describe the characteristics of supercapacitors; however, it is difficult to apply as it is to circuit simulation tools such as the Professional Simulation Program with Integrated Circuit Emphasis (PSPICE), PSIM, and Matlab/Simulink. First, as shown in Fig. 12, the impedance of the porous electrode can be explained as a CPE and ZARC elements connected in series as the parallel circuit of R_n-$\mathrm{CPE_{pore}}$ [24], and the parameters of the circuit can be represented as follows:

$$R_n = \frac{2R_e}{n^2\pi^2}, \quad \mathrm{CPE} = \frac{1}{(j\omega)^d Q_d}, \mathrm{CPE_{pore}} = \frac{2}{(j\omega)^d Q_d}$$

where $n = 1, 2, 3, \ldots$

When the unit current step is applied to the ZARC element, its voltage response in the time domain can be expressed as (9) [22]. However, not only is (9) complicated and difficult to interpret, but predefined elements are not available in commercially available software such as PSPICE, PSIM, and Matlab/Simulink. Thus, mathematical approximation of the ZARC element is essential for the integrated simulation of a supercapacitor and a power electronic system.

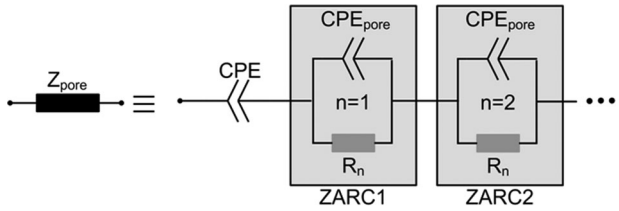

Fig. 12. Equivalent impedance model of porous electrode.

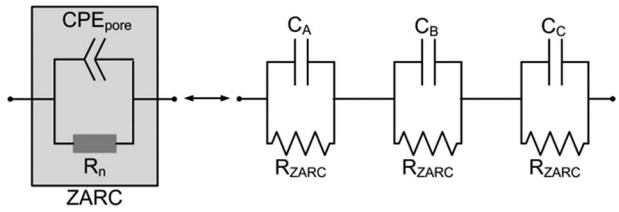

Fig. 13. Equivalent impedance model of ZARC element.

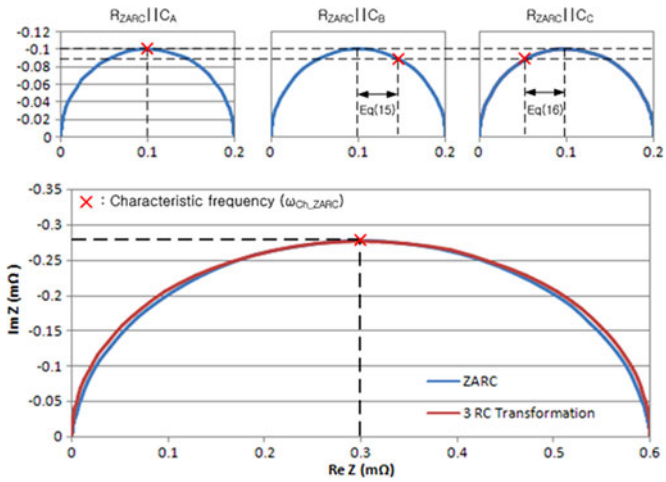

Fig. 14. Transformation of ZARC element to three *R-C* parallel circuits.

$$v_{\mathrm{ZARC}}(t) = R_n\left[\sum_{i=1}^{\infty}(-1)^{i-1}\frac{1}{R_n Q_d}\cdot\frac{t^{id}}{\Gamma(1+id)}\right] \tag{9}$$

In this paper, three *R-C* parallel circuits were used in the approximation, since it has been already demonstrated that this number provides sufficient accuracy of approximation as well as reasonable computation time, as shown in Fig. 13 [24]. Fig. 14 shows how the ZARC element can be approximated by several *R-C* parallel circuits connected in series. The approximation can be achieved by determining the real and imaginary components of the three *R-C* parallel circuits such that the summation of the real and imaginary components of each *R-C* circuit have the same values as the real and imaginary components of the ZARC element at the characteristic frequency ($\omega_{\mathrm{ch\_ZARC}}$) for which the imaginary component is smallest. The characteristic frequency of the ZARC element ($\omega_{\mathrm{ch\_ZARC}}$) can be calculated by equating the real component of the ZARC element in (10) to $R_n/2$, as is expressed in (11). In addition, the imaginary value of the ZARC element [$\mathrm{Im(ZARC)_{ch}}$] at the characteristic frequency can be calculated

according to (12)

$$\mathrm{ZARC} = \frac{R_n}{1+(j\omega)^d R_n Q_d} = \frac{R_n\{1+\omega^d R_n Q_d \cos(d\pi/2)\} - j\omega^d R_n^2 Q_d \sin(d\pi/2)}{1+2\omega^d R_n Q_d \cos(d\pi/2)+\omega^{2d} R_n^2 Q_d^2} \tag{10}$$

$$\omega_{\mathrm{ch\_ZARC}} = \left(\frac{1}{R_n Q_d}\right)^{1/d} \tag{11}$$

$$\mathrm{Im(ZARC)}_{\omega_{\mathrm{ch\_ZARC}}} = -\frac{R_n \cdot \sin(d\pi/2)}{2\{1+\cos(d\pi/2)\}}. \tag{12}$$

First, the resistance of each *R-C* parallel circuit is equally given as 1/3 of R_n, the resistance of the ZARC element, so that the summation of the real components of the three *R-C* parallel circuits is the same as the real component of the ZARC element. Using this resistance value and the characteristic frequency obtained from (11), the capacitance C_A can be calculated as (13). However, if the same capacitance value is applied to the other two *R-C* circuits, the resulting impedance plot of the three *R-C* circuits cannot form a depressed semicircle on the complex plane. Thus, the capacitances C_B and C_C have to be adjusted using $f(d)$, a function of the d parameter of the CPE element, as shown in (14).

$$C_A = \frac{1}{\omega_{\mathrm{ch\_ZARC}} \cdot R_n/3} \tag{13}$$

$$C_B = \frac{C_A}{f(d)}, \quad C_C = C_A \times f(d). \tag{14}$$

If the capacitance C_B and C_C are adjusted by (14), the geometrical positions of the impedances of the $R_{\mathrm{ZARC}}\|C_B$ and $R_{\mathrm{ZARC}}\|C_C$ circuits on the Nyquist impedance plot at the characteristic frequency ($\omega_{\mathrm{ch\_ZARC}}$) move to the right and left with reference to the vertex of the semicircle, respectively, as shown in Fig. 14. On the real axis, the geometrical distances between the vertex and each impedance of $R_{\mathrm{ZARC}}\|C_B$ and $R_{\mathrm{ZARC}}\|C_C$ circuits at the characteristic frequency ($\omega_{\mathrm{ch\_ZARC}}$) can be expressed as (15) and (16), respectively, and are the same in the magnitude regardless of the value of f(d). Therefore, the real component of the three *R-C* parallel circuits is equal to 3/2 R_{ZARC} as expressed by (17). Table III gives the real and imaginary components of the three *R-C* parallel circuits, equivalently transformed to a ZARC element at the characteristic frequency ($\omega_{\mathrm{ch\_ZARC}}$).

$$R_{\mathrm{ZARC}}/2 - \mathrm{Re}(R_{\mathrm{ZARC}} \parallel C_B)_{\omega_{\mathrm{ch\_ZARC}}} = \frac{R_{\mathrm{ZARC}} - R_{\mathrm{ZARC}} f(d)^2}{2(1+f(d)^2)} \tag{15}$$

$$R_{\mathrm{ZARC}}/2 - \mathrm{Re}(R_{\mathrm{ZARC}} \parallel C_C)_{\omega_{\mathrm{ch\_ZARC}}} = \frac{R_{\mathrm{ZARC}} - R_{\mathrm{ZARC}} f(d)^2}{2(1+f(d)^2)} \tag{16}$$

$$\mathrm{Re}(R_{\mathrm{ZARC}} \parallel C_A)_{\omega_{\mathrm{ch\_ZARC}}} + \mathrm{Re}(R_{\mathrm{ZARC}} \parallel C_B)_{\omega_{\mathrm{ch\_ZARC}}} + \mathrm{Re}(R_{\mathrm{ZARC}} \parallel C_C)_{\omega_{\mathrm{ch\_ZARC}}} = \frac{3}{2} R_{\mathrm{ZARC}}. \tag{17}$$

TABLE III
FITTED THE EQUATION OF RE Z AND IM Z FOR EACH *R-C* PARALLEL CIRCUITS AT THE CHARACTERISTIC FREQUENCY

	$R_{ZARC}\|C_A$	$R_{ZARC}\|C_B$	$R_{ZARC}\|C_C$
RE Z_{CH}	$\frac{R_{ZARC}}{2}$	$\frac{R_{ZARC} f(d)^2}{1+f(d)^2}$	$\frac{R_{ZARC}}{1+f(d)^2}$
Im Z_{ch}	$\frac{-R_{ZARC}}{2}$	$\frac{-R_{ZARC} f(d)}{1+f(d)^2}$	$\frac{-R_{ZARC} f(d)}{1+f(d)^2}$

TABLE IV
FUNCTION $f(d)$ FOR THE TRANSFORM OF THREE *R-C* PARALLEL CIRCUITS

Parameter "d"	f(d)
1.0	1
0.95	1.697
0.9	2.181
0.85	2.714
0.8	3.354
0.75	4.160
0.7	5.218

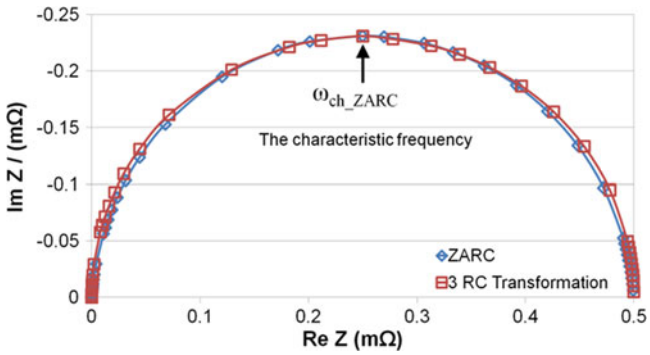

Fig. 15. Nyquist impedance plots of ZARC and its equivalent model.

As shown in Table III, the imaginary component of the $R_{\mathrm{ZARC}}\|C_A$ circuit has a value of $-R_{\mathrm{ZARC}}/2$, whereas the imaginary components of the $R_{\mathrm{ZARC}}\|C_B$ and $R_{\mathrm{ZARC}}\|C_C$ circuits are larger, thereby forming a depressed semicircle on the complex plane. Thus, the relationship between the summation of the imaginary components of all three *R-C* parallel circuits and the function *f(d)* is expressed by (18).

$$\mathrm{Im}(R_{\mathrm{ZARC}} \parallel C_A)_{\omega_{\mathrm{ch\_ZARC}}} + \mathrm{Im}(R_{\mathrm{ZARC}} \parallel C_B)_{\omega_{\mathrm{ch\_ZARC}}} + \mathrm{Im}(R_{\mathrm{ZARC}} \parallel C_C)_{\omega_{\mathrm{ch\_ZARC}}} = -\frac{R_{\mathrm{ZARC}}}{2}\left(1+\frac{4f(d)}{1+f(d)^2}\right). \tag{18}$$

The function *f(d)* can be derived by equating (12) to (18), as shown in (19). Table IV gives the calculated values of *f(d)* for different values of *d*.

$$f(d) = \frac{-2+\sqrt{4-\beta}}{\beta} \quad \beta = \frac{3\sin(d\pi/2)}{1+\cos(d\pi/2)} + 1. \tag{19}$$

Fig. 15 shows that the Nyquist impedance plot of the ZARC element, when $R_n = 0.5$ mΩ, $Q_d = 3000$, and $d = 0.95$, is the same as that of the three *R-C* parallel circuits transformed

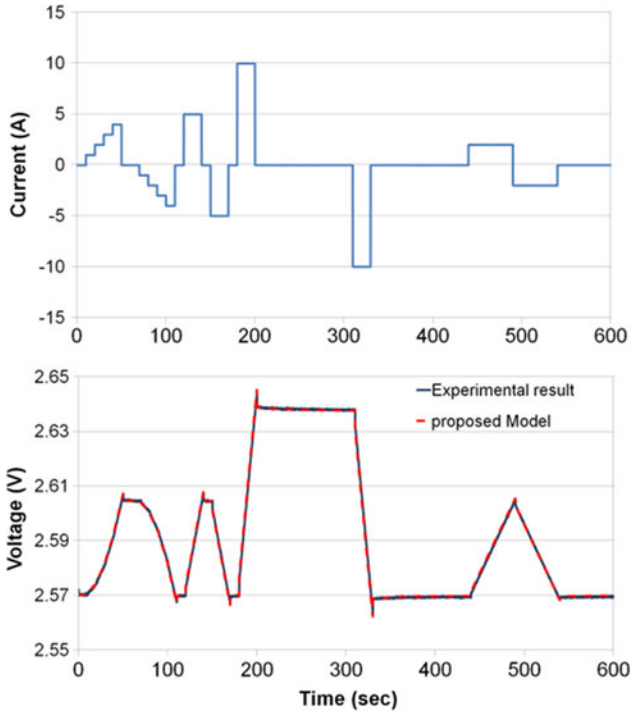

Fig. 16. Comparison between measured voltage and simulated voltage for different load currents.

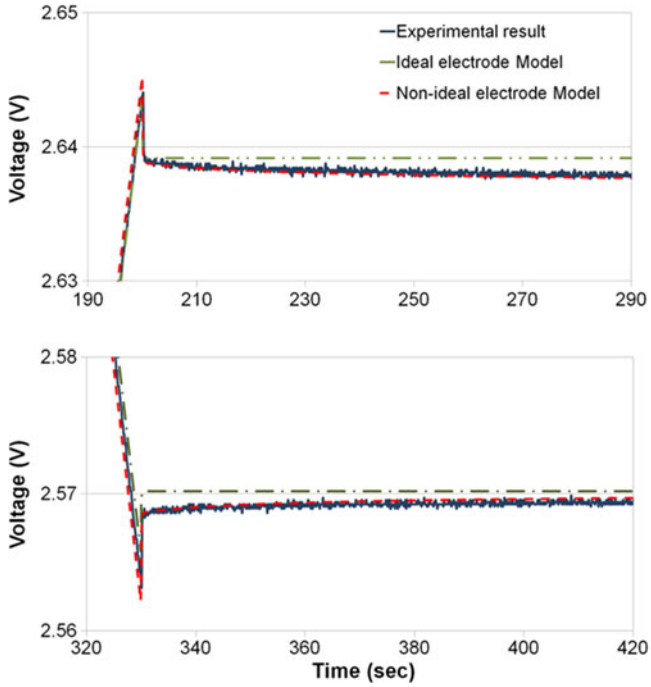

Fig. 17. Comparison between simulation results obtained using conventional and proposed models and experimental results.

equivalently from the ZARC element, which implies that the two models have the same characteristics.

To verify the accuracy and validity of the proposed model, the equivalent circuit of the supercapacitor was simulated with Matlab/Simulink. Fig. 16 illustrates the charge/discharge current of a step function, which was realized by applying an input signal generated by LabVIEW to the external control terminal of the BP4610 bipolar power supply and measuring the terminal voltage of the supercapacitor as the response voltage. Long pause periods were inserted in the waveform of the load current from 200 to 310 s and from 330 to 440 s to observe the effect of self-discharge, and the same waveform of current was applied in the Matlab/Simulink simulation. The simulation results were compared with the experimental results. As shown in Fig. 16, the results of the simulation with the nonideal electrode agreed well with those of the experiment.

In Fig. 17, the waveform of the response voltage of the supercapacitor, when there was cut-off of current at 200 and 330 s, as shown in Fig. 16, was compared with the results of the simulation employing the ideal and nonideal electrode models. The simulation with the nonideal electrode model was found to provide results more similar to the waveform of the experiment than the simulation with the ideal electrode model provided. Accordingly, it was found that the equivalent impedance model of the supercapacitor involving a nonideal electrode model can precisely explain self-discharge arising after the cut-off of charge current and instant recharge after the cut-off of discharge current.

VI. Conclusion

In this study, the nonideal porous electrode structure of a supercapacitor, with a CPE, was modeled and a method for the precise dynamic simulation of the supercapacitor that takes into consideration self-discharge and variations in parameters was proposed. The method employed the impedance model developed taking into consideration the physical structure of the supercapacitor and the movement of ions within. The methods could accurately represent the dynamic characteristics of supercapacitors, i.e., self-discharge after charge and instant reverse charging after discharge. The proposed method of modeling and simulation helps simulate a supercapacitor with a power electronic circuit and, thus, makes it possible to predict accurately dynamic features of the supercapacitor. It is thus expected that the method will be useful in designing cost-effective and high-performance power electronics systems employing supercapacitors.

References

[1] E. Faggioli, P. Rena, V. Danel, X. Andrieu, R. Mallant, and H. Kahlen, "Supercapacitors for the energy management of electric vehicles," *J. Power Sources*, vol. 84, pp. 261–269, 1999.

[2] A. D. Pasquier, I. Plitz, S. Menical, and G. Amatucci, "Supercapacitors for the energy management of electric vehicles," *J. Power Sources*, vol. 115, pp. 171–178, 2003.

[3] J. N. Marie-Francoise, H. Gualous, R. Outbib, and A. Berthon, "42 V Power Net with supercapacitor and battery for automotive applications," *J. Power Sources*, vol. 143, pp. 275–283, 2005.

[4] P. Thounthong, S. Rael, and B. Davat, "Control strategy of fuel cell and supercapacitors association for a distributed generation system," *IEEE Trans. Ind. Electron*, vol. 54, no. 6, pp. 255–3233, Dec. 2007.

[5] S. Kim and S. Sul, "Control of rubber tyred gantry crane with energy storage based on supercapacitor bank," *IEEE Trans. Power Electron.*, vol. 21, pp. 1420–1427, Sep. 2006.

[6] A. Payman, S. Pierfederici, and F. M. Tabar, "Energy management in a fuel cell/supercapacitor multisource/multiload electrical hybrid system," *IEEE Trans. Power Electron.*, vol. 24, pp. 2681–2691, Dec. 2009.
[7] H. Chen, B. Wei, and D. Ma, "Energy storage and management system with carbon nanotube supercapacitor and multidirectional power delivery capability for autonomous wireless sensor nodes, *IEEE Trans. Power Electron.*, vol. 25, pp. 2897–2909, Dec. 2010, 2011.
[8] S. Buller, E. Karden, D. Kok, and R. W. De Doncker, "Modeling the dynamic behavior of supercapacitors using impedance spectroscopy," *IEEE Trans. Ind. Applicat*, vol. 38, no. 6, pp. 1622–1626, Nov./Dec. 2002.
[9] L. Zubieta and R. Bonert, "Characterization of double-layer capacitors for power electronics applications," *IEEE Trans. Ind. Electron*, vol. 36, no. 1, pp. 199–205, Jan./Feb. 2000.
[10] B. E. Conway, *Electrochemical Supercapacitor: Scientific Principles and Technological Applications.*. New York: Plenum, 1999.
[11] F. Rafik, H. Gualous, R. Gallay, A. Crausaz, and A. Berthon, "Frequency, thermal and voltage supercapacitor characterization and modeling," *J. Power Sources*, vol. 165, pp. 928–934, 2007.
[12] Y. Diab, P. Venet, H. Gualous, and G. Rojat, "Self-discharge characterization and modeling of electrochemical capacitor used for power electronics applications," *IEEE Trans. Power Electron.*, vol. 24, pp. 510–517, Feb. 2009.
[13] M. Kaus, J. Kowal, and D. U. Sauer, "Modelling the effects of charge redistribution during self-discharge of supercapacitors," *Electrochimica Acta*, vol. 55, pp. 7516–7523, 2010.
[14] R. De Levie, *Electrochemical Response of Porous and Rough Electrodes, Advances in Electrochemistry and Electrochemical Engineering*. vol. 6, New York: Wiley Interscience, 1967.
[15] O. Bohlen, J. Kowal, and D. U. Sauer, "Ageing behaviour of electrochemical double layer capacitors Part I. Experimental study and ageing model," *J. Power Sources*, vol. 172, pp. 468–475, 2007.
[16] O. Bohlen, J. Kowal, and D. U. Sauer, "Ageing behaviour of electrochemical double layer capacitors Part II. Lifetime simulation model for dynamic applications," *J. Power Sources*, vol. 173, pp. 626–632, 2007.
[17] J. Lee and W. Choi, "Development of the low-cost impedance spectroscopy system for modeling the electrochemical power sources," *The 7th ICPE*, pp. 113–118, Oct. 2007.
[18] *NF BP4610 Instruction Manual,* NF Corp., Yakohama: Japan, 2005.
[19] *NI 6124 /6154 User Manual,* Nat. Instruments Corp., Austin, TX, 2008.
[20] H. Gualous, D. Bouquain, A. Berthon, and J. M. Kauffmann, "Experimental study of supercapacitor serial resistance and capacitance variations with temperature," *J. Power Sources*, vol. 123, pp. 86–93, 2003.
[21] H. E. Brouji, J-M. Vinassa, O. Briat, N. Bertrand, and E. Woirgard, "Ultracapacitors self discharge modelling using a physical description of porous electrode impedance," in *Proc. IEEE Vehicles Power Propul. Conf.*, Harbin, China, 3–5 Sep. 2008.
[22] A. Salkind, T. Atwater, P. Singh, S. Nelatury, S. Damodar, C. Fennie, Jr., and D. Reisner, "Dynamic characterization of small lead-acid cells," *J. Power Sources*, vol. 96, pp. 151–159, 2001.
[23] J. Kowal, E. Avaroglu, F. Chamekh, A. Senfelds, T. Thien, D. Wijaya, and D. Sauer, "Detailed analysis of the self-discharge of supercapacitors," *J. Power Sources*, 2009.
[24] S. Buller, Impedance-based simulation models for energy storage devices in advanced automotive power systems, Ph.D. dissertation, Inst. for Power Electron. and Electr. DrivesISEA, RWTH Aachen Univ., 2002.

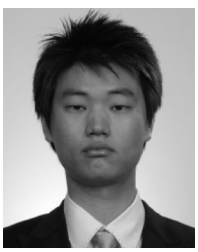

Sang-Hyun Kim was born in Seoul, Korea, in 1981. He received the B.S. and M.S. degrees in electrical engineering from the Soongsil University, Seoul Korea, in 2008 and 2010, respectively.

He is currently a Research Engineer of the Power Electronics Technology Team, POSCOICT, Seoul, Korea. His research interests include energy storage systems and grid-connected inverters.

Woojin Choi (S'00–M'05) was born in Seoul, Korea, in 1967. He received the B.S. and M.S. degrees in electrical engineering from the Soongsil University, Seoul, Korea, in 1990 and 1995, respectively, and the Ph.D. degree in electrical engineering from Texas A&M University, College Station, TX, in 2004.

From 1995 to 1998, he was a Research Engineer at the central R&D division of Daewoo Heavy Industries. Since 2005, he has been with the School of Electrical Engineering, Soongsil University, where he is an Associate Professor. He is an Associate Editor of the *Journal of Power Electronics*. His current research interests include modeling and control of electrochemical energy sources, such as fuel cells, batteries and supercapacitors, power conditioning technologies in renewable energy systems, dc.-dc converters for fuel cell and hybrid electric vehicles and charging infrastructure for the smart grid.

Kyo-Beum Lee (S'02–M'04–SM'10) was born in Seoul, Korea, in 1972. He received the B.S. and M.S. degrees in electrical and electronic engineering from the Ajou University, Korea, in 1997 and 1999, respectively, and the Ph.D. degree in electrical engineering from the Korea University, Korea, in 2003.

From 2003 to 2006, he was with the Institute of Energy Technology, Aalborg University, Aalborg, Denmark. From 2006 to 2007, he was with the Division of Electronics and Information Engineering, Chonbuk National University, Jeonju, Korea. Since 2007, he has been with the Division of Electrical and Computer Engineering as an Associate Professor in Ajou University. He is an Associate Editor of the IEEE TRANSACTIONS ON POWER ELECTRONICS and the *Journal of Power Electronics*. His research interests include electric machine drives and renewable power generations.

Sewan Choi (S'92–M'96–SM'04) received the B.S. degree in electronic engineering from Inha University, Incheon, Korea, in 1985 and the M.S. and Ph.D. degrees in electrical engineering from Texas A&M University, College Station, TX, in 1992 and 1995, respectively.

From 1985 to 1990, he was with Daewoo Heavy Industries as a Research Engineer. From 1996 to 1997, he was a Principal Research Engineer at Samsung Electro-Mechanics Co., Korea. In 1997, he joined the Department of Control and Instrumentation Engineering, Seoul National University of Science and Technology (Seoul Tech), Seoul, Korea, where he is currently a Professor. His research interests include power conversion technologies for renewable energy systems and energy storage systems and DC-DC converters and battery chargers for electric vehicles. He is an Associate Editor of the IEEE TRANSACTIONS ON POWER ELECTRONICS and IEEE TRANSACTIONS ON INDUSTRY APPLICATIONS.